Materials and Structures (2021) 54:102
https://doi.org/10.1617/s11527-021-01699-6

ORIGINAL ARTICLE

The load-bearing behaviour of a reinforced concrete beam investigated by optical measuring techniques

Götz Hüsken · Stephan Pirskawetz · Detlef Hofmann · Frank Basedau · Klaus-Peter Gründer · Daniel Kadoke

Received: 29 September 2020 / Accepted: 28 March 2021 / Published online: 19 April 2021

Abstract Bending beams and slabs are typical examples for structural elements used for reinforced concrete structures such as bridge girders, T-beams and bridge decks. Their strength related failure modes at maximum loading can be divided into bending and shear failure. The failure of beams loaded in bending can occur with or without indication. Therefore, conventional design concepts aim on failure modes with sufficient indication (e.g. large deflections or cracks), as it occurs in the case of secondary flexural compression failure. These indicating factors can also be used for Structural Health Monitoring (SHM) of civil infrastructure systems (e.g. bridges) to identify structural changes. In this context, non-destructive testing (NDT) methods offer different techniques for measuring deflections or crack formation and opening. However, profound knowledge on the determining failure modes of bending beams and their detection by NDT methods is required for the reliable application of SHM. Different NDT methods have been used in this study for analysing the load-bearing behaviour of a reinforced concrete beam in bending. The different measuring techniques are briefly described and their applicability is discussed by means of experimental results. For this purpose, the load-bearing behaviour of a reinforced concrete beam having a span of 2.75 m was investigated in a four-point bending flexural test at laboratory scale. The focus is on the characterization of determining failure modes by optical NDT and the comparison with classical measuring techniques (e.g. deformation measurements by displacement transducers). The bending beam was equipped with two single-mode (SM) sensor fibres. One fibre served as Distributed Optical Fibre Sensor (DOFS), whereas the other fibre contained Fibre Bragg Grating (FBG) sensors. In addition, optical deformation measurements using Digital Image Correlation (DIC) and Stereophotogrammetry (SP) were conducted.

Keywords Concrete beam · Bending · Digital image correlation · Stereophotogrammetry · Distributed fibre optic sensor · Fibre bragg grating

1 Introduction

A detailed analysis of bridges in the German trunk road network reveals that in 2016 the condition of about 55 % of the 39 000 bridges can be classified as ‘very good’, ‘good’ or ‘satisfactory’ [1]. However, the remaining 45 % are classified as ‘sufficient’ (33 %), ‘poor’ (11 %) and ‘deficient’ (1 %). Depending on their condition, repair measures have to be performed in the near future or on short-term in the case of ‘sufficient’ and ‘poor’ condition, respectively [2].

G. Hüsken (✉) · S. Pirskawetz · D. Hofmann · F. Basedau · K.-P. Gründer · D. Kadoke
Bundesanstalt für Materialforschung und -prüfung (BAM), Unter den Eichen 87, 12205 Berlin, Germany
e-mail: goetz.huesken@bam.de

Extensive repair measures or new construction of the bridge is necessary if the condition is classified as 'deficient'. However, the decision-making process in terms of repair or reconstruction of the damaged structure requires detailed information on the remaining static and dynamic load-bearing behaviour of the bridge and their condition. For this purpose, Structural Health Monitoring (SHM) is a useful tool for evaluating the condition of bridges or other structural elements exposed to bending loads.

Relevant loads leading to the degradation of bridges are caused by combinations of mechanical, thermal, hygric and chemical influences. Therefore, various systems and sensors are available for monitoring the condition of engineering structures and which allow the monitoring of the structural behaviour, corrosion behaviour of the reinforcement and relevant concrete parameters such as temperature, water content, pH value, chloride content, carbonation, etc. Essential information on changes in the structural behaviour can be obtained by measuring deformations of structural elements – both length changes and deflections – crack widths and accelerations [3, 4].

Length changes or deformations of structural elements are usually measured by Linear Variable Differential Transformers (LVDTs), extensometers or strain gauges. These sensors allow a precise but discreet measurement of deformations in a very defined and usually small area. Information on the overall load-bearing behaviour of an entire beam cannot be obtained by these classical measuring techniques. However, if this information is needed, fibre optic sensors or photogrammetric measuring methods must be used. The successful application of these systems for testing reinforced concrete is reported manifold in literature for fibre optic sensors [5–20] and photogrammetric measuring methods [21–23], respectively.

The most valuable and promising application in SHM is the use of Distributed Optical Fibre Sensors (DOFS) as these sensors allow for continuous measurements in different directions of structural members. This way, the global behaviour can be monitored with reasonable accuracy. Laboratory investigations comprise the application of DOFS in tensile tests on isolated reinforcing bars [13], on reinforcing bars embedded in concrete [13, 15, 17, 18], sensor fibres applied on the concrete surface [13, 16, 17] or embedded in the concrete [19]. Furthermore, a comprehensive overview on the use of fibre optic sensors, both distributed fibre optic strain measurements as well as discrete systems, is presented by Regier and Hoult [9] for load tests conducted on a reinforced concrete bridge. The experimental investigations conducted by Brault and Hoult [15, 16] as well as Poldon et al. [18] are combined with Digital Image Correlation (DIC), which allows the measurement of crack width on the concrete surface. However, profound knowledge on the determining failure modes and their characterization by different measuring systems is required for an appropriate interpretation of the measured data in terms of SHM. This implies also the combination and synchronization of different systems such as optical and acoustic measuring techniques.

The required techniques and methods for condition analysis and condition monitoring of bridges were investigated by using a bridge demonstrator that was built as reference structure. The bridge demonstrator is a two-span beam with a span of 12 m in each segment and was tested using both destructive and non-destructive measuring techniques. In preparation of these field tests, the application, handling, and synchronization of various measuring systems was tested on smaller specimens on laboratory scale. The results of these preliminary tests obtained by optical measuring techniques, such as photogrammetric measurements and fibre optic sensors are discussed and compared with classical measuring techniques.

2 Experimental program

2.1 Test setup

2.1.1 Beam design

A reinforced concrete beam was designed according to DIN EN 1992-1-1 (Eurocode 2) [24] without partial safety factors for material properties and actions, respectively. The beam was designed for the resulting moment in a four-point bending test considering the boundary conditions of the available test machine in terms of maximum load (100 kN) and maximum span (3 m). The resulting static system is given in Figure 1.

A reference concrete C(0.45) with 16 mm maximum aggregate size according to DIN EN 1766 [32] was used for casting the beam. Compressive and

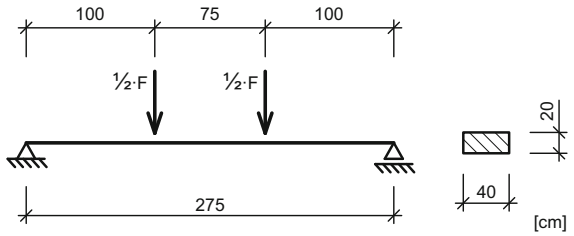

Fig. 1 Static system and cross section of the beam

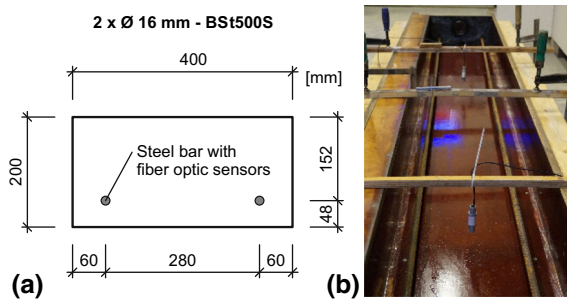

Fig. 2 Bending beam: **a** Position of the steel bars; **b** Mould before casting of the beam

flexural strength of the concrete mix used was determined on reference samples and amounts to 65.4 MPa and 4.1 MPa, respectively. The mix proportioning and further material properties used for the beam design are given in Table 1. The cross section of the beam was given with 40 cm in width and 20 cm in height. The reinforcement of the beam was realized by two reinforcing bars BSt500S with 16 mm diameter resulting in a cross section A_s of 4.02 cm^2. Upper reinforcement was not needed as the beam was designed for pure bending failure without concrete crushing in the compression zone. Considering these boundary conditions, the yield strength of the reinforcement is reached at approx. 60 kN. Figure 2 shows the position of the reinforcement of the beam and the casting of the corresponding beam.

The beam was designed without shear reinforcement to avoid a reduction of the concrete cross section around the stirrups and hence to avoid predefined cracking in these areas. The calculated shear force of the beam at maximum load is lower than the calculated shear force capacity without stirrups ($V_{Ed} \leq V_{Rd,c}$). Undesired shear failure will, therefore, not occur.

2.1.2 *Loading and data acquisition*

Structural elements like bridge girders are designed to carry imposed loads and their self-weight over a wide span. This results in nearly constant tensile stresses over long distances in the tension zone. To induce a comparable load in the laboratory experiment, the beam was subjected to a four-point bending test, which results in a constant bending moment in the middle section of the beam without shear forces.

The beam span was 275 cm provided by two supports on the load frame base of the servo-hydraulic testing machine. A stiff crossbeam transmitted the force of a hydraulic actuator, integrated in the upper cross-head of the machine, to the two loading pins on the upper surface of the beam. The loading pins had a span of 75 cm. To avoid unexpected movements or sudden failure of the beam, the load was applied with a constant displacement rate (see Fig. 3). Control variable was the piston stroke which was measured by a displacement transducer installed in the hydraulic

Table 1 Mix design and concrete properties

Material	Amount (kg/m^3)	Parameter	Value
CEM I 42.5R	375.0	Flow table test - DIN EN 12350-5 [25] (mm)	510
Quarz sand 0–0.5	236.0	Fresh concrete density - DIN EN 12350-6 [26] (kg/m^3)	2401
Quarz sand 0.5–1.0	145.0	Air content - DIN EN 12350-7 [27] (%)	0.9
Quarz sand 1.0–2.0	163.0	Density of hardened concrete - DIN EN 12390-7 [28] (kg/m^3)	2359
Quarz sand 2.0-4.0	254.0	Compressive strength - DIN EN 12390-3 [29] (MPa)	65.4±0.9
Gravel 4-8	327.0	Flexural strength - DIN EN 12390-5 [30] (MPa)	4.1±0.3
Gravel 8-16	690.0	Modulus of elasticity - DIN EN 12390-13 [31] (GPa)	35.2±0.8
Water reducer	5.63		
Water	169.0		

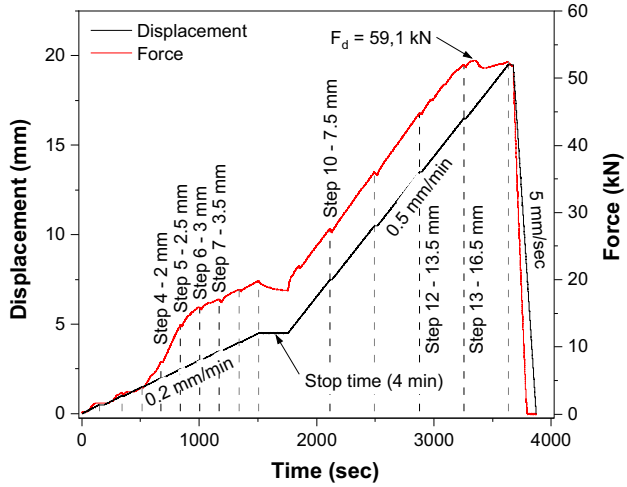

Fig. 3 Loading rate, resulting force, and loading steps. The loading steps highlighted in black correspond to the measuring intervals of the DOFS that are discussed in detail

actuator. The resulting force was measured by a 100 kN load cell mounted between the crossbeam and the piston rod. The deformation of the beam was measured between the lower surface of the beam and the load frame base of the machine by three LVDTs. Two transducers were positioned directly next to the bearings and one in the middle of the beam (see Fig. 4). This way, possible influences from deformations of the load frame or supports are corrected.

After applying a pre-load of 0.25 kN and offset correction of the displacement transducers and the load cell, a first measurement of the photogrammetric measuring systems and the fibre optic sensors was conducted by a manually sent trigger. This first measurement serves as reference for the following measurements. Further measurements of the DIC system were conducted by automatic trigger signals that were sent from the servo-hydraulic testing machine in intervals of about 5 seconds. Additionally, the measured force was transmitted to the DIC system by a voltage signal. The FBG system allows the measurement with a constant sampling frequency of 10 Hz.

A low displacement rate of 0.2 mm/min was applied at the beginning to study the formation of micro cracks in detail. Both photogrammetric measuring systems were therefore triggered every 0.013 mm of piston displacement. Since the distributed optical fibre sensors (DOFS) require a measuring time of about 3 seconds, an additional dwell time of about 20 seconds was inserted every 0.5 mm of piston displacement. After transition from the non-cracked to the cracked state, the displacement rate was increased to 0.5 mm/min. The time between the trigger signals

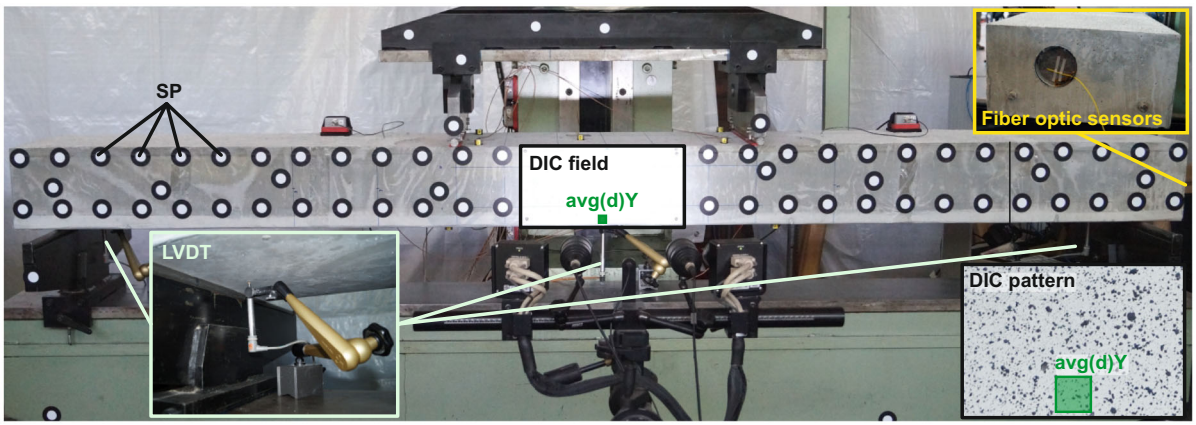

Fig. 4 Beam installed in the testing machine and applied measuring systems

correlates now with a piston displacement of 0.033 mm. The measurement of the DOFS was conducted in this stage every 3 mm of piston displacement. After yielding of the reinforcing bars was detected, the beam was unloaded with 6 mm/sec to prevent rupture of the reinforcing bars and resulting damage of the sensors. The entire loading and the beam's response are shown in Fig. 3. No fibre measurements were taken in the unloading phase, but all other measuring systems were still active.

2.2 Photogrammetric measuring methods

Two photogrammetric measuring systems were used for analysing the deformation of the loaded beam. The two photogrammetric systems used are based on stereo camera arrangements for 3D coordinate determination by means of spatial triangulation of high-contrast surface features of the test specimen [33, 34]. An exact determination of the spatial orientation of the two cameras relative to each other and the parameters of each camera, taking into account i.e. sensor and image imperfections, are requirements for a high degree of coordinate accuracy. This process is commonly referred to as system calibration. Changes on the camera system that can affect the parameters mentioned before have to be avoided.

2.2.1 Digital image correlation

Digital image correlation (DIC) is one photogrammetric measuring method that was applied in the midsection of the beam to analyse the formation and propagation of cracks. The corresponding DIC field having an area of about 200 mm by 400 mm is shown in Fig. 4. The camera arrangement observes a high-contrast stochastic pattern. DIC allows individual tracking of the movement of small sub-areas having a size of e.g. 20 x 20 pixels within the stochastic pattern at all loading conditions. The coordinate changes of the sub-areas can either be used to analyse the crack opening or strain values can be derived which enable crack visualization in terms of strain concentrations.

2.2.2 Stereophotogrammetry

The second photogrammetric measuring method that was used for the bending test is stereophotogrammetry (SP). This method observes the entire front side of the beam and focuses on high-contrast circular markers that are visible in Fig. 4. The circular markers are both located on the beam surface and the load transmitting crossbeam as well as the machine foundation for control purpose. The 3D center coordinates of the circular markers are used to compute the 3D components of the associated displacement vectors for all loading conditions. This way, the total deflection of the beam and the corresponding bending line can be derived.

2.3 Fibre optic sensors

Two single-mode (SM) sensor fibres were glued over the entire length of one reinforcing bar of the beam for determining the progression of the strain distribution and resulting cracks during the four-point bending test. The fibres were protected by an epoxy coating and protruding from both ends of the beam. Figure 5 shows the position of the different sensor fibres. One fibre served as sensor fibre for distributed strain measurements. For this purpose, a standard SM fibre (SMF-28e) according to DIN EN 60793-2-50 [35] was used. The second fibre contains a Fibre Bragg Grating (FBG) array consisting of five recoated FBG sensors with different Bragg wavelengths for continuous local strain measurement according to DIN EN 61757-1-1 [36]. The two fibre optic measurement methods used for the sensor fibres complement and reference each other.

2.3.1 Distributed fibre optic sensors

A LUNA Optical Backscatter Reflectometer (LUNA OBR 4600) was used as a measuring system for distributed strain measurements. The strain

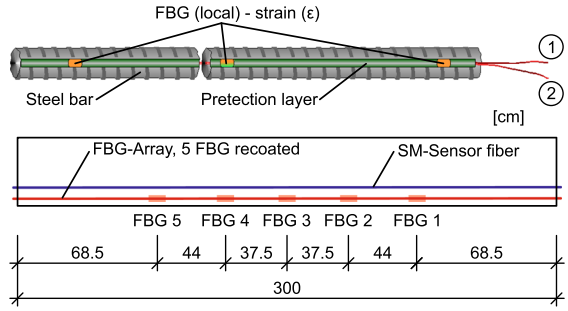

Fig. 5 Schematic illustration of the applied fibre optic sensors and their positions along the reinforcing steel bar

measurement is based on the evaluation of Rayleigh scattering in the fibre. The principle of a swept-wavelength interferometer (SWI) is used to obtain a high-resolution backscattering profile along the measurement path by analysing the complex amplitude and phase information in the frequency domain and transforming it into the local domain. If the obtained data are correlated to a reference measurement, the result represents the distributed strain or temperature change of the fibre. Distributed sensing achieves a local resolution of ±1.0 cm/m and a strain resolution of ±1.0 µm/m.

2.3.2 *Fibre bragg grating*

Fibre Bragg Gratings (FBG) are periodic refractive index changes written into an optical fibre that form an interference filter. The FBG reflects light of a specific wavelength. Deformation of the Bragg grating changes the grating period and thus also the Bragg wavelength. A FBG interrogator HBM DI 410 was used for the measurement. This instrument is a 4-channel, long-term stable, calibration-capable multi-channel measuring system with integrated reference source for FBG sensors. The interrogator couples the light of a tunable laser into the sensor fibre. If the coupled wavelength and Bragg wavelength of an FBG are identical, the light reflected by the FBG is detected by a photodetector. The signals are further processed in the interrogator and made available as wavelength or strain values. The device allows sampling rates up to 1 kHz with a repeatability of 1 pm (equivalent to approx. 1 µm/m strain) for wavelength ranging from 1510 nm to 1590 nm.

3 Results and discussion

Figure 6 shows the load-deflection behaviour of the beam determined by the two photogrammetric measuring systems (DIC, SP) and the LVDT installed in the middle of the beam. A sub area with a side length of 10 mm was defined in the lower middle section of the DIC field for calculating the beam deflection as arithmetic mean avg(d)Y of the corresponding surface component (see Fig. 4). The lower two markers that are close to the DIC field have been used for calculating the beam deflection of the corresponding force-deflection plot depicted in Fig. 6.

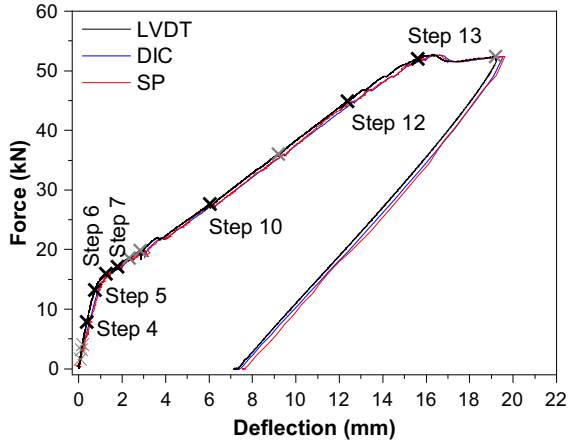

Fig. 6 Force-deflection plots of the tested beam determined by the different measuring systems. The loading steps highlighted in the graph correspond to the measuring intervals of the DOFS depicted in Fig. 3

The comparison of the data reveals that the deformation behaviour was determined with low deviation. The difference of the beam deflection measured by the three different systems is lower than 0.3 mm at maximum load. The force-deflection plot shows three distinct phases that correspond to the load-bearing behaviour known from literature [37]. At small loads, such as Step 4, the tensile stresses are carried proportionally by both the non-cracked concrete and the reinforcement. The beam behaves like a homogeneous member and stresses and strains are linearly distributed over the entire cross section. This initial phase is followed by the transition from the non-cracked to the cracked state. The resulting tensile stresses in the bottom of the beam exceed the tensile strength of the concrete and cracks begin to develop in this phase (Step 5 to Step 6). The cracks grow quickly with increasing load (Step 7) and the neutral axis moves upwards until the reinforcement starts to yield and the ultimate load of the beam is reached in the final phase. A detailed analysis of the different phases is given in the following sections for the NDT methods used.

3.1 Photogrammetric measuring methods

The results of the DIC measurements are depicted in Fig. 7 for relevant steps of the force-deflection plot. Step 5 in Fig. 7 shows the formation of cracks in the bottom of the beam as indicated by local strain

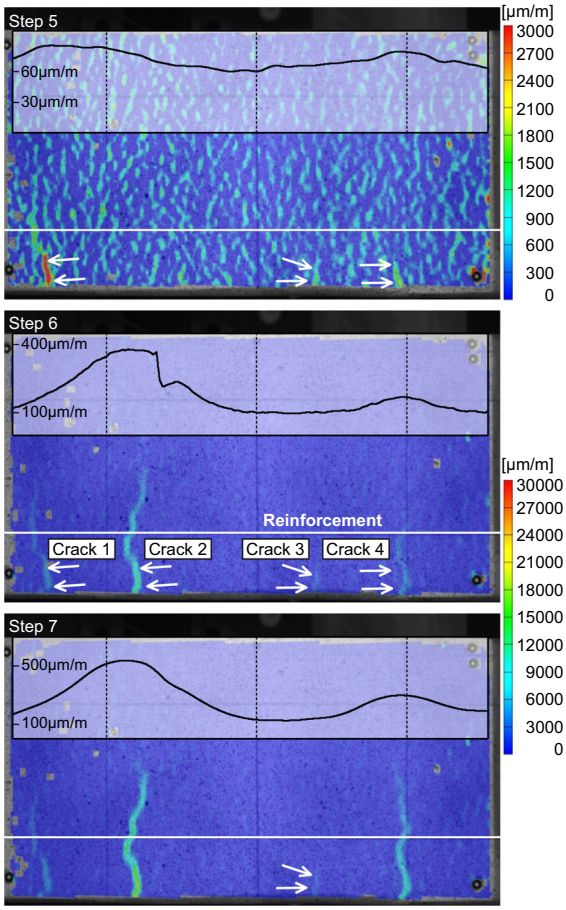

Fig. 7 Strain distribution in the DIC field at the loading steps highlighted in Figs. 3 and 6, respectively. The graphs in the upper part of the corresponding sub-pictures show the strains measured by the DFOS on the reinforcement

concentrations. Although slightly higher strain values have been determined by the DFOS in the corresponding areas of the reinforcement, the formed cracks are below the reinforcement in the observation area of the DIC system. This fact can be attributed to both, the resolution of the DIC system and the irregular crack pattern inside the beam. The initially formed cracks grow with increasing load and the strain values measured by the DFOS become more distinct in the corresponding areas as the cracks are now exceeding the reinforcement (see Step 6 in Fig. 7). At this stage, 4 cracks with different crack length are visible in the measuring field of the DIC. However, the further crack opening is not equal. It is evident from Figs. 7 and 8 that Crack 2 shows the largest crack length and width at Step 6. With increasing load,

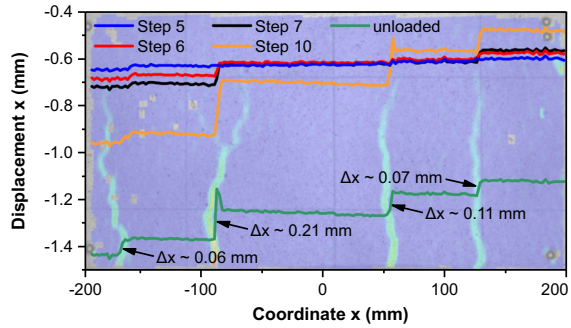

Fig. 8 Horizontal displacement of the beam in the bottom section of the DIC field indicating the crack width. The diagram is underlaid with strain distribution in the DIC field determined at Step 10

Crack 4 shows a clear increase in both crack length and width at Step 7, while Crack 1 and Crack 2 reveal no significant changes. A clear opening of Crack 3 becomes obvious at the loading level obtained at Step 10, but Crack 1 shows still the lowest crack width at this stage (see Fig. 8). The difference in the crack opening determined at Step 10 by the DIC system corresponds also with the crack width of the unloaded beam, indicating the remaining plastic deformations after testing the beam. Here, Crack 2 shows the largest crack width at Step 10 and after testing.

The overall deformation of the beam was captured by SP. The results are depicted in Fig. 9 for the deformation of the beam at maximum load and in Fig. 10 for the remaining deformation after unloading the beam. The displacement vectors show the vertical displacement of the corresponding markers. As mentioned before, the deviation of the beam deflection determined by SP and LVDT in the midsection is small (see Fig. 6). Considering the static system of the beam depicted in Fig. 1 and a possible rotation of the

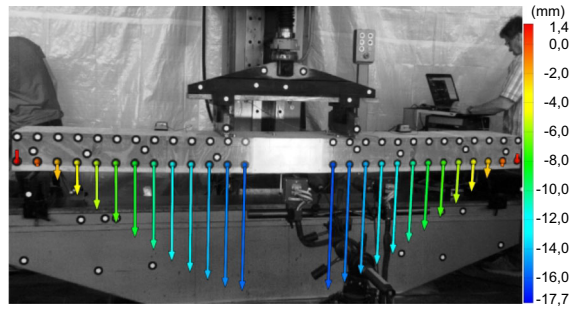

Fig. 9 Deflection of the beam at maximum load determined using SP

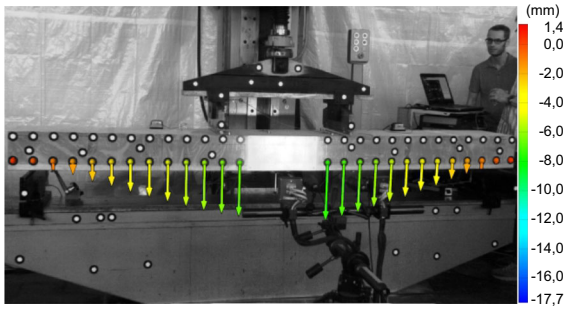

Fig. 10 Remaining deflection of the beam after unloading determined using SP

beam at the supports, the ends of the beam have to moved upward during the bending test. It was possible to register this upward movement with the SP system and the corresponding vertical displacement of the outer circular markers is about 1.4 mm.

3.2 Fibre optic sensors

The strain distribution of the reinforcement determined by DFOS is shown in Fig. 11 for different loading steps. Step 4 shows the strain distribution for a small load in the non-cracked state. As mentioned, the beam shows a homogeneous behaviour for small loads and stresses and strains are linearly distributed over the entire cross section. At this state, the tensile strain of the concrete does not exceed the limiting tensile strain, which is given with 100 µm/m to 120 µm/m [38]. Therefore, the strain distribution of the reinforcement corresponds to the bending line of the beam.

First cracks are formed during the transition from the non-cracked (Step 4) to the cracked state (Step 5) when the resulting tensile stresses in the bottom of the beam exceed the tensile strength of the concrete. At Step 5 slightly higher strain values have been determined between the loading pins indicating the formation of first cracks. These initially formed cracks grow with increasing load (Step 6 to Step 13), which results in higher local strain values of the reinforcement due to the crack opening near the reinforcement. With increasing load (Step 7 to Step 13) cracks outside the loading pins are formed and the area of cracked concrete extends towards the bearings. The reinforcement shows locally plastic deformations when the maximum load (Step 13) is reached. These local

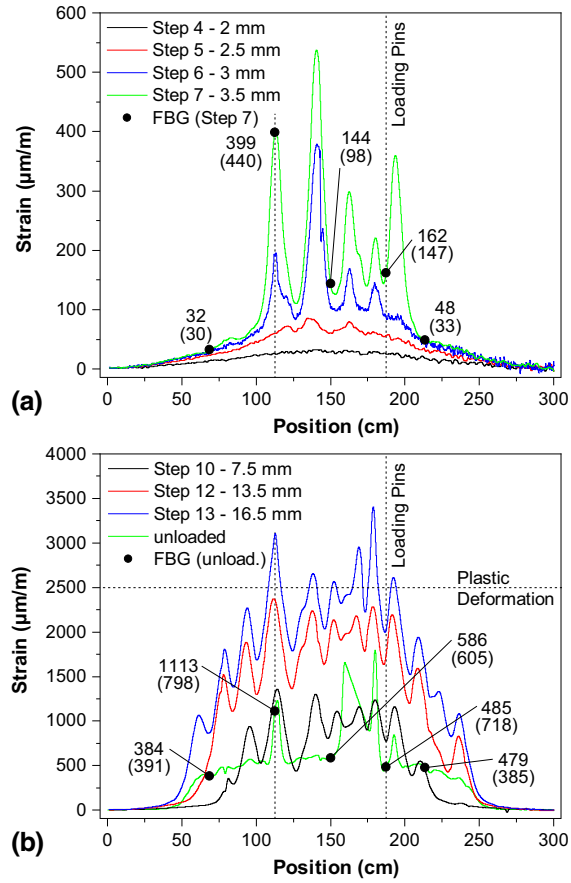

Fig. 11 Strain distribution of the reinforcement determined by DFOS at different loading steps highlighted in Figs. 3 and 6, respectively. The position of the FBG sensors is marked and the corresponding values of the DFOS and FBG sensors are given (values of the FBG sensors are given in brackets)

plastic deformations remain as characteristic peaks of the strain plot of the unloaded beam (see Fig. 11b).

Strains measured by the FBGs are plotted over time versus the applied displacement and the resulting force in Fig. 12. Furthermore, the position of the FBGs is marked in Fig. 11 and the corresponding strain values for Step 7 (Fig. 11a) and the unloaded beam (Fig. 11b) are given in brackets in comparison to the local strain values measured by the DFOS. Additional values are given in Table 2. Both measuring systems show a rather good agreement in their measured values for the beam in the non-cracked state (up to Step 4). However, with the transition from the non-cracked to the cracked state (Step 5), the deviation between both systems increases differently. Large deviations of single values can be attributed to the fact that the correct positioning

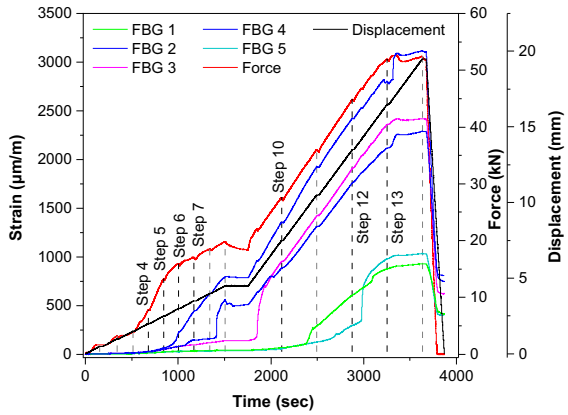

Fig. 12 Strains over time measured by the FBG sensors as well as force and displacement measured by the testing machine, respectively

of the FBGs is decisive for measurements conducted on the reinforcement near local strain peaks, such as cracks. Here, a difference in the position of the FBG sensor of about 0.5 mm in combination with the limited local resolution of the distributed sensing (DFOS) can result in a large difference of the measured strain values. Similar observations for strain measurements in the vicinity of cracks have also been reported by Regier and Hoult [9].

The influence of cracks on the different measuring systems is also evident from the data depicted in Fig. 12. Here, FBG sensors located in an area with later crack formation (e.g. FBG 1 and FBG 5) show similar strain values until a crack is formed in the surrounding area of the sensor and the corresponding strain value shows a large increase. This can either be a rapid and sudden increase (e.g. FBG 2) in case the crack crosses the FBG sensor directly and which corresponds to the resulting theoretical local strain increase in the crack or a continuous and smooth increase (e.g. FBG 1) if the FBG sensor is located close to the formed crack, but not directly in the crack. Similar findings have been described by Brault and Hoult [15]. The rapid strain increase measured by an FBG sensor on the reinforcement and directly crossed by a crack in the concrete turns to a continuous increase once the crack crosses the reinforcement completely. The further continuous strain increase of the reinforcement in the crack is proportional to the applied loading rate.

Table 2 Strain values measured by Fibre Bragg Grating (FBG) and Distributed Optical Fibre Sensor (DOFS) at different loading steps

Loading	Strain (µm/m)									
Step	FBG 1	DFOS	FBG 2	DFOS	FBG 3	DFOS	FBG 4	DFOS	FBG 5	DFOS
1	2	3	4	4	4	6	5	4	2	2
2	5	4	9	6	9	9	10	9	5	7
3	6	9	12	13	12	17	13	13	6	7
4	13	18	25	25	24	29	29	26	12	15
5	23	32	52	57	52	61	66	60	22	23
6	31	47	81	86	79	104	223	192	27	26
7	33	48	147	162	98	144	440	399	30	32
8	38	59	158	300	119	231	624	754	33	38
9	41	74	549	469	140	447	797	912	36	42
10	68	455	886	775	953	865	1357	1305	56	64
11	290	942	1311	1197	1417	1320	1925	1823	126	193
12	608	1224	1761	1756	1910	2023	2424	2362	294	587
13	878	1609	2116	2032	2359	2414	2798	3096	981	868
14	929	1691	2291	2062	2420	2342	3120	3399	1034	907
unloaded	385	479	718	485	605	586	798	1113	391	384

4 Conclusions

The load-bearing behaviour of a reinforced concrete beam was investigated by optical measuring techniques and compared with results obtained by classical measuring techniques. The use of two different systems for optical deformation measurements (Digital Image Correlation (DIC) and Stereophotogrammetry (SP)) showed good results for determining the deflection of a bending beam. The deflection of the beam was determined by both systems with low deviation compared to classical measurements conducted with Linear Variable Differential Transformers (LVDTs). The DIC system allows also for determining the planar strain distribution of the tested samples, which helps to characterise and to analyse the crack formation and crack propagation in concrete beams.

The application of fibre optic sensors proved to be a useful investigation tool for characterizing the load-bearing behaviour of a reinforced concrete beam. Distributed Optical Fibre Sensor (DOFS) and Fibre Bragg Grating (FBG) sensors were applied on the reinforcement of the concrete beam to determine the strain distribution during the four-point bending flexural test. Here, local strains can be determined with high accuracy and high measuring frequency by FBG sensors, whereas DOFS allow continuously distributed measurements along the reinforcement with lower accuracy and lower measuring frequency.

The results obtained by the laboratory test on a reinforced concrete beam showed that optical measuring systems are suitable tools for Structural Health Monitoring (SHM). The three-dimensional detection of deformations and resulting strains with optical deformation measurements is beneficial for analysing the damage mechanism of loaded structures and related crack formation. Comparable results can hardly be obtained by classical measuring techniques or, if possible, extensive technical efforts are necessary. The same holds for strain measurements using fibre optic sensors. Here, the application of DOFS for determining the strain distribution along the reinforcement offers new possibilities for SHM that cannot be realized with classical measuring systems such as strain gauges.

Acknowledgements This study was undertaken as part of the BLEIB project within the Federal Institute for Materials Research and Testing (BAM) and funded by the Federal Ministry for Economic Affairs and Energy (BMWi), Germany.

Funding Open Access funding enabled and organized by Projekt DEAL.

Declarations

Conflict of interest The authors declare that they have no conflict of interest.

References

1. BMVI (2016) Stand der Ertüchtigung der Straßenbrücken im Bestand der Bundesfernstraßen *Bericht zur Vorlage an den Ausschuss für Verkehr, Bau und Stadtentwicklung des Deutschen Bundestages*. 14 November 2016
2. BRH (2015) Erhaltungsbedarfsprognose im Bundesfernstraßenbau *Bericht an den Haushaltsausschuss des Deutschen Bundestages*. 22 May 2015
3. Raupach M, Büttner T (2014) Concrete repair to EN 1504: diagnosis, design, principles and practice. CRC Press, London
4. Comisu CC, Taranu N, Boaca G, Scutaru MC (2017) Structural health monitoring system of bridges. Procedia Eng 199:2054–2059. https://doi.org/10.1016/j.proeng.2017.09.472
5. Leung C (2001) Fiber optic sensors in concrete: the future? NDT E Int 34(2):85–94. https://doi.org/10.1016/s0963-8695(00)00033-5
6. Habel WR (2003) Faseroptische Sensoren für hochaufgelöste Verformungsmessungen in der Zementsteinmatrix. Forschungsbericht 246, Bundesanstalt für Materialforschung und -prüfung (BAM), Berlin, Germany
7. Schallert M, Habel WR, Göbel IR, Stahlmann J, Wardinghus P (2008) Dynamic and static testing of concrete foundation piles with structure-integrated fiber optic sensors. In: Santos JA (ed) Stress Wave – 8th International Conference on the Application of Stress-wave Theory to Piles, 8-10 September 2008, Lisbon, Portugal, pp 625–634
8. Kesavan K, Ravisankar K, Parivallal S, Sreeshylam P, Sridhar S (2010) Experimental studies on fiber optic sensors

embedded in concrete. Measurement 43(2):157–163. https://doi.org/10.1016/j.measurement.2009.08.010
9. Regier R, Hoult NA (2014) Distributed strain behavior of a reinforced concrete bridge: case study. J Bridge Eng. https://doi.org/10.1061/(asce)be.1943-5592.0000637
10. Bremer K, Wollweber M, Weigand F, Rahlves M, Kuhne M, Helbig R, Roth B (2016) Fibre optic sensors for the structural health monitoring of building structures. Procedia Technol 26:524–529. https://doi.org/10.1016/j.protcy.2016.08.065
11. Kindler A, Schaber MB, Glötzl J, Brentle J, Lieh A (2016) Nachweis der Ankertragfähigkeit am Beispiel eines innovativen Ankermonitorings. In: Aubram D (ed) Vorträge zum 12. Hans Lorenz Symposium, Technische Universität Berlin, 6 October 2016, Berlin, Germany, pp 69–84
12. Brandes K, Daum W, Hofmann D, Basedau F, Kubowitz P (2016) Innovative structural damage detection of bridges by least squares adjustment with constraints. Mater Today Proc 3(4):942–946. https://doi.org/10.1016/j.matpr.2016.03.025
13. Barrias A, Casas J, Villalba S (2018) Embedded distributed optical fiber sensors in reinforced concrete structures - a case study. Sensors 18(4):980. https://doi.org/10.3390/s18040980
14. Liehr S, Münzenberger S, Krebber K (2018) Wavelength-scanning coherent OTDR for dynamic high strain resolution sensing. Optics Exp 26(8):10573–10588. https://doi.org/10.1364/oe.26.010573
15. Brault A, Hoult N (2019a) Distributed reinforcement strains: measurement and application. ACI Struct J 116(4):115–127. https://doi.org/10.14359/51714483
16. Brault A, Hoult N (2019b) Monitoring reinforced concrete serviceability performance using fiber-optic sensors. ACI Struct J 116(1):57–70. https://doi.org/10.14359/51710870
17. Nurmi S, Hoult NA, Howell SD (2019) Distributed strain monitoring of two-way slabs. Eng Struct 189:580–588. https://doi.org/10.1016/j.engstruct.2019.04.002
18. Poldon JJ, Hoult NA, Bentz EC (2019) Distributed sensing in large reinforced concrete shear test. ACI Struct J 116(5):235–245. https://doi.org/10.14359/51716765
19. Bassil A, Wang X, Chapeleau X, Niederleithinger E, Abraham O, Leduc D (2019) Distributed fiber optics sensing and coda wave interferometry techniques for damage monitoring in concrete structures. Sensors 19(2):356. https://doi.org/10.3390/s19020356
20. Heidenreich F, Herten M, Hofmann D, Basedau F (2020) Verwendung faseroptischer Messtechnik im Zuge wiederholter Eignungsprüfungen an Verpressankern. In: Messen in der Geotechnik 2020, Technische Universität Braunschweig, pp 297–324, https://doi.org/10.24355/dbbs.084-201912181435-0
21. Jiang R, Jáuregui DV, White KR (2008) Close-range photogrammetry applications in bridge measurement: literature review. Measurement 41(8):823–834. https://doi.org/10.1016/j.measurement.2007.12.005
22. Valença J, da Costa DD, Júlio E, Araújo H, Costa H (2013) Automatic crack monitoring using photogrammetry and image processing. Measurement 46(1):433–441. https://doi.org/10.1016/j.measurement.2012.07.019
23. Carmo R, Valença J, Silva D, da Costa DD (2015) Assessing steel strains on reinforced concrete members from surface cracking patterns. Constr Build Mater 98:265–275. https://doi.org/10.1016/j.conbuildmat.2015.08.079
24. Fingerloss F, Hegger J, Zilch K (2012) Eurocode 2 für Deutschland: DIN EN 1992-1-1 Bemessung und Konstruktion von Stahlbeton- und Spannbetontragwerken - Teil 1–1: Allgemeine Bemessungsregeln und Regeln für den Hochbau mit Nationalem Anhang. Beuth Verlag GmbH, Berlin, Germany
25. DIN EN 12350-5 (2009) Testing fresh concrete – Part 5: Flow table test; German version EN 12350-5:2009. Deutsches Institut für Normung e.V
26. DIN EN 12350-6 (2011) Testing fresh concrete – Part 6: Density; German version EN 12350-6:2009. Deutsches Institut für Normung e.V
27. DIN EN 12350-7 (2009) Testing fresh concrete – Part 7: Air content - Pressure methods; German version EN 12350-7:2009. Deutsches Institut für Normung e.V
28. DIN EN 12390-7 (2009) Testing hardened concrete – Part 7: Density of hardened concrete; German version EN 12390-7:2009. Deutsches Institut für Normung e.V
29. DIN EN 12390-3 (2009) Testing hardened concrete – Part 3: Compressive strength of test specimens; German version EN 12390-3:2009 . Deutsches Institut für Normung e.V
30. DIN EN 12390-5 (2009) Testing hardened concrete – Part 5: Flexural strength of test specimens; German version EN 12390-5:2009. Deutsches Institut für Normung e.V
31. DIN EN 12390-13 (2014) Testing hardened concrete – Part 13: Determination of secant modulus of elasticity in compression; German version EN 12390-13:2013. Deutsches Institut für Normung e.V
32. DIN EN 1766 (2017) Products and systems for the protection and repair of concrete structures – Test methods - Reference concretes for testing; German version EN 1766:2017. Deutsches Institut für Normung e.V
33. Atkinson KB (ed) (1996) Close range photogrammetry and machine vision. Whittles Publishing, Scotland
34. Sharpe WN (ed) (2008) Springer handbook of experimental solid mechanics. Springer, US, New York
35. DIN EN 60793-2-50 (2016) Optical fibres – Part 2-50: Product specifications - Sectional specification for class B single-mode fibres (IEC 60793-2-50:2015). Deutsches Institut für Normung e.V
36. DIN EN 61757-1-1 (2017) Fibre optic sensors – Part 1-1: Strain measurement - Strain sensors based on fibre Bragg gratings (IEC 61757-1-1:2016). Deutsches Institut für Normung e.V
37. Zilch K, Zehetmaier G (2010) Bemessung im konstruktiven Betonbau, 2nd edn. Springer, Berlin, Germany
38. Leonhardt F (1988) Cracks and crack control in concrete structures. PCI J 33(4):124–145. https://doi.org/10.15554/pcij.07011988.124.145